

Fixing the Scale and Shift in Monocular Depth For Camera Pose Estimation

Yaqing Ding¹, Václav Vávra¹, Viktor Kocur², Jian Yang³, Torsten Sattler⁴, and Zuzana Kukelova¹

¹ Visual Recognition Group, Faculty of Electrical Engineering, Czech Technical University in Prague

² Faculty of Mathematics, Physics and Informatics, Comenius University in Bratislava

³ PCA Lab, Nanjing University of Science and Technology, Nanjing, China

⁴ Czech Institute of Informatics, Robotics and Cybernetics, Czech Technical University in Prague

Abstract

Recent advances in monocular depth prediction have led to significantly improved depth prediction accuracy. In turn, this enables various applications to use such depth predictions. In this paper, we propose a novel framework for estimating the relative pose between two cameras from point correspondences with associated monocular depths. Since depth predictions are typically defined up to an unknown scale and shift parameter, our solvers jointly estimate both scale and shift parameters together with the camera pose. We derive efficient solvers for three cases: (1) two calibrated cameras, (2) two uncalibrated cameras with an unknown but shared focal length, and (3) two uncalibrated cameras with unknown and different focal lengths. Experiments on synthetic and real data, including experiments with depth maps estimated by 11 different depth predictors, show the practical viability of our solvers. Compared to prior work, our solvers achieve state-of-the-art results on two large-scale, real-world datasets. The source code is available at https://github.com/yaqding/pose_monodepth

1. Introduction

Camera pose estimation is a core problem in a wide range of computer vision applications, including Structure-from-Motion (SfM) [53], visual localization [51, 57, 63], and autonomous robots [41]. Typically, camera poses are estimated from correspondences between images and / or 3D scene models, usually established using feature matching. The type of camera pose estimation problem depends on the type of correspondences available: (i) Given 2D-2D matches between a pair of images, the relative pose [25, 35, 37, 46, 55, 56] between the two images can be estimated based on the epipolar geometry [26]. (ii) Given 3D-2D correspondences between 3D scene points and 2D image pixels, the absolute pose of the image can be esti-

mated relative to a known 3D model of scene by solving a PnP problem [20]. (iii) Given 3D-3D correspondences between 3D scene points, the relative pose between both point sets (and thus, by extension between images observing the sets) can be computed [1, 22].

For two calibrated cameras, the relative pose can be estimated from 5 point correspondences using the well-known 5-point algorithm [25, 35, 46, 56] (or using 4 point correspondences to estimate a homography [26] in the case of planar scenes). If the focal length is unknown, but both cameras share the same focal length, the relative pose can be estimated together with the focal length from 6 point correspondences [25, 35, 37, 55]. If the full intrinsic calibration is unknown and/or both cameras have different calibrations, the relative pose can be estimated from 7- or 8-point correspondences [26].

A 2D-3D correspondence provides more constraints (2) compared to a 2D-2D correspondence (1 constraint). Thus, absolute pose estimation algorithms typically require fewer correspondences than relative pose estimation ones. For example, the absolute pose of a calibrated camera can be estimated from three 2D-3D correspondences via a P3P algorithm [15, 20, 32, 33, 47, 48]. Four point correspondences are sufficient to jointly estimate the pose and an unknown focal length parameter [10, 36, 40, 60].

A single 3D-3D correspondences provides 3 constraints on the alignment of two sets of points. Still, three 3D-3D correspondences are needed to compute the relative pose aligning two sets of points (as using only two correspondences leads to a remaining degree of freedom (DoF), namely a rotation around the line connecting the two points in a point set). At the same time, 3D points typically have different noise characteristics than 2D points, *i.e.*, an optimal alignment in 3D does not necessarily correspond to an optimal alignment according to the 2D measurements. Furthermore, 3D data is generally noisier than 2D image features [52]. Consequently, 3D-3D correspondences are typically not used to solve camera pose estimation problems.

Algorithms for camera pose estimation problems are

usually employed in RANSAC-style hypothesize-and-verify frameworks [18] in order to handle outlier correspondences. The number of RANSAC iterations grows exponentially with outlier ratio, *i.e.*, the ratio of wrong correspondences among all correspondences, and the number of correspondences needed to estimate the pose. As such, a considerable amount of works focus on reducing the number of correspondences necessary for pose estimation, typically by using additional information such as the gravity direction from an Inertial Measurement Unit (IMU) [19, 34, 45, 58], or information about the local feature geometry such as scale and rotation [3, 24, 43] or local affine frames [5, 6, 17]. *E.g.*, [2] proposed a closed-form solution to the relative pose of two calibrated cameras that makes use of the fact that relative depths can be estimated from feature scales. They developed a neural network to estimate the relative scale of the features.

Recently, learning-based methods [9, 21, 27, 44, 49, 59, 61, 62] have achieved significant success in monocular depth estimation. These methods typically produce affine-invariant monocular depth or inverse depth, meaning that the estimated depth or inverse depth is defined up to an unknown scale factor and shift. Incorporating additional information from monocular depth offers further constraints for geometric problems. In the most closely related work, [16] assumes that the shift in monocular depth can be disregarded and proposes new solvers that use relative depth for fundamental matrix estimation. Their solvers are unaffected by the scale of the monocular depth.

Inspired by advancements in monocular depth estimation, this paper presents a comprehensive discussion on camera pose estimation using monocular depth in two cameras. Specifically, we account for both the scale and shift of the monocular depth and propose new formulations that simultaneously estimate the relative pose of two cameras along with the scale and shift parameters of the monocular depths. The main contributions of the paper are:

- We integrate scale and shift of monocular depth into camera pose estimation, thus formulating a problem of their joint estimation.
- We discuss all the possible cases for different camera configurations, and propose new minimal solvers for calibrated cameras, two cameras with equal and unknown focal length, and two cameras with varying focal lengths.
- In extensive real and synthetic experiments, we show an improvement in terms of accuracy and speed over the existing solvers.

2. Problem Statement

Assume that a set of 3D points Ω is observed by two cameras with projection matrices $\mathbf{K}_1[\mathbf{I} \mid \mathbf{0}]$ and $\mathbf{K}_2[\mathbf{R} \mid \mathbf{T}]$. Let $\{\mathbf{p}_i, \mathbf{q}_i\}, i = 1, \dots, n$ be a set of n 2D point correspondences, *i.e.*, the projections of 3D points Ω in the first and

the second camera, respectively. Then we have

$$\lambda_i \mathbf{K}_2^{-1} \mathbf{q}_i = \eta_i \mathbf{R} \mathbf{K}_1^{-1} \mathbf{p}_i + \mathbf{T}, \quad (1)$$

where λ_i and η_i are the depths of the points \mathbf{q}_i and \mathbf{p}_i , respectively. Recently, several learning-based methods [21, 61] that provide non-metric monocular depth estimates, *i.e.*, the depth estimates with unknown scale factor and shift, have been proposed. Using these methods, we can obtain a depth image corresponding to the RGB image.

A depth image can provide additional information for camera pose estimation. In this paper, we study, how such monocular depth known up to scale and shift [61, 62] can be used in pose estimation of two cameras. Our goal is to estimate the scale, shift, and motion parameters simultaneously.

3D-3D Solver Modeling Scale and Shift.

Modern learning based monocular depth estimation can provide affine invariant depth [31, 44, 59] or affine invariant inverse depth [61, 62].

i) Depth up to scale and shift.

The true depths λ_i and η_i in (1) can be expressed as

$$\eta_i = s_1(\alpha_i + u), \quad \lambda_i = s_2(\beta_i + v), \quad (2)$$

where α_i, β_i are estimated depths up to scale and shift, and $\{s_1, s_2\}, \{u, v\}$ are the unknown scales and shifts of the depths. Substituting (2) into (1), we have

$$s_2(\beta_i + v) \mathbf{K}_2^{-1} \mathbf{q}_i = s_1(\alpha_i + u) \mathbf{R} \mathbf{K}_1^{-1} \mathbf{p}_i + \mathbf{T}, \quad (3)$$

Dividing (3) by s_1 , we have

$$s(\beta_i + v) \mathbf{K}_2^{-1} \mathbf{q}_i = (\alpha_i + u) \mathbf{R} \mathbf{K}_1^{-1} \mathbf{p}_i + \mathbf{t}, \quad (4)$$

where $s = s_2/s_1$ and $\mathbf{t} = \mathbf{T}/s_1$. Note that in this case, the scale of the translation \mathbf{t} is defined w.r.t. s_1 , thus we can not further fix the scale of \mathbf{t} , *i.e.* the translation vector is not estimated up to scale like in the standard relative pose solvers [46], but needs to be estimated as a 3 degrees of freedom (3-DOF) vector.

This means that for calibrated cameras, *i.e.*, for the known \mathbf{K}_1 and \mathbf{K}_2 , we have a 9-DOF problem w.r.t. $\{s, u, v, \mathbf{R}, \mathbf{t}\}$. Since one 3D-3D point correspondence provides three constraints of the form (4), we need at least 3 point correspondences with their monocular depths to solve this problem for the calibrated case. For the case of unknown focal lengths f_1 and f_2 in calibration matrices \mathbf{K}_1 and \mathbf{K}_2 , we have 10 and 11 DoF, for cases $f_1 = f_2$ and $f_1 \neq f_2$ respectively.

ii) Inverse Depth up to scale and shift.

In this case, the true depths can be expressed as

$$\eta_i = \frac{s_1}{\alpha_i + u}, \quad \lambda_i = \frac{s_2}{\beta_i + v}, \quad (5)$$

E Solver	Point Correspondence			Scale Ratio	Shift	DOF	No. of Solutions
	3D-3D	3D-2D	2D-2D				
5-point [46]	-	-	5	-	-	5	10
Rel3PT [2]	2	-	1	1	(0, 0)	5	4
P3P [15]	-	3	-	1	(0, -)	6	4
3PT ₁₀₀	1	1	1	1	(0, 0)	6	4
3PT _{1uu}	1	2	0	1	(u, u)	7	8
3PT _{1uv}	2	1	0	1	(u, v)	8	8
3PT _{s00}	1	2	0	s	(0, 0)	7	4
3PT _{suu}	2	1	0	s	(u, u)	8	8
3PT _{svu}	3	0	0	s	(u, v)	9	4
3PT _{svv} (inverse)	3	0	0	s	(u, v)	9	10

Table 1. Different combinations of using 3D-3D, 3D-2D and 2D-2D point correspondences for calibrated camera pose estimation.

where α_i, β_i are known values from the inverse monocular depth, and $\{s_1, s_2\}, \{u, v\}$ are the unknown scales and shifts in the inverse depth. Substituting (5) into (1), we have

$$\frac{s_2}{\beta_i + v} \mathbf{K}_2^{-1} \mathbf{q}_i = \frac{s_1}{\alpha_i + u} \mathbf{R} \mathbf{K}_1^{-1} \mathbf{p}_i + \mathbf{T}, \quad (6)$$

Dividing (6) by s_1 , we have

$$\frac{s}{\beta_i + v} \mathbf{K}_2^{-1} \mathbf{q}_i = \frac{1}{\alpha_i + u} \mathbf{R} \mathbf{K}_1^{-1} \mathbf{p}_i + \mathbf{t},. \quad (7)$$

In this case, we again have 9 DOF for calibrated cameras. However, in contrast to the previous case, the constraints (7) are more complex, since they contain unknown parameters in the denominators.

In some scenarios, we may have some additional information about the scale and shift $\{s, u, v\}$, e.g., assuming zero shift or equal scale. There are 6 possible cases of combinations of known and unknown shifts and scales (see Table 1) resulting in different DoF problems. Note that, although one 3D-3D point correspondence provides three constraints, we can not use only two 3D-3D point correspondences to solve 6-DOF pose problem with known $\{s, u, v\}$. The reason is the rotation can not be determined with only two points. There still remains 1-DOF rotation around the line passing through the two points. Due to the space limitation, we only discuss the 9-DOF problem w.r.t. $\{s, u, v, \mathbf{R}, \mathbf{t}\}$ in the main paper. Other cases are shown in the appendices.

3. Calibrated Camera Pose Estimation

In this section, we first discuss the calibrated case where the camera intrinsic parameters are known, i.e., the calibration matrices \mathbf{K}_1 and \mathbf{K}_2 are known from calibration or EXIF. We use $\tilde{\mathbf{q}}_i = \mathbf{K}_2^{-1} \mathbf{q}_i$, $\tilde{\mathbf{p}}_i = \mathbf{K}_1^{-1} \mathbf{p}_i$ to represent the normalized image points.

3.1. Depth up to Scale and Shift

Given 3 point correspondences and their monocular depths, substituting $\tilde{\mathbf{q}}_i, \tilde{\mathbf{p}}_i, i = 1, 2, 3$ into (4) we have nine equa-

tions in nine unknowns

$$s(\beta_i + v) \tilde{\mathbf{q}}_i = (\alpha_i + u) \mathbf{R} \tilde{\mathbf{p}}_i + \mathbf{t}, \quad (8)$$

$$s(\beta_i + v) \tilde{\mathbf{q}}_i = (\alpha_i + u) \mathbf{R} \tilde{\mathbf{p}}_i + \mathbf{t}, \quad (9)$$

$$s(\beta_i + v) \tilde{\mathbf{q}}_i = (\alpha_i + u) \mathbf{R} \tilde{\mathbf{p}}_i + \mathbf{t}. \quad (10)$$

By eliminating the translation from the above equations, i.e., by subtracting pairs of equations (8)-(9), (8)-(10), and (9)-(10) we have

$$s(\beta_1 + v) \tilde{\mathbf{q}}_1 - s(\beta_2 + v) \tilde{\mathbf{q}}_2 = \mathbf{R}((\alpha_1 + u) \tilde{\mathbf{p}}_1 - (\alpha_2 + u) \tilde{\mathbf{p}}_2),$$

$$s(\beta_1 + v) \tilde{\mathbf{q}}_1 - s(\beta_3 + v) \tilde{\mathbf{q}}_3 = \mathbf{R}((\alpha_1 + u) \tilde{\mathbf{p}}_1 - (\alpha_3 + u) \tilde{\mathbf{p}}_3),$$

$$s(\beta_2 + v) \tilde{\mathbf{q}}_2 - s(\beta_3 + v) \tilde{\mathbf{q}}_3 = \mathbf{R}((\alpha_2 + u) \tilde{\mathbf{p}}_2 - (\alpha_3 + u) \tilde{\mathbf{p}}_3).$$

Since applying the rotation matrix on a vector preserves the length of this vector, we have the following constraints

$$\|s(\beta_1 + v) \tilde{\mathbf{q}}_1 - s(\beta_2 + v) \tilde{\mathbf{q}}_2\| = \|(\alpha_1 + u) \tilde{\mathbf{p}}_1 - (\alpha_2 + u) \tilde{\mathbf{p}}_2\|,$$

$$\|s(\beta_1 + v) \tilde{\mathbf{q}}_1 - s(\beta_3 + v) \tilde{\mathbf{q}}_3\| = \|(\alpha_1 + u) \tilde{\mathbf{p}}_1 - (\alpha_3 + u) \tilde{\mathbf{p}}_3\|,$$

$$\|s(\beta_2 + v) \tilde{\mathbf{q}}_2 - s(\beta_3 + v) \tilde{\mathbf{q}}_3\| = \|(\alpha_2 + u) \tilde{\mathbf{p}}_2 - (\alpha_3 + u) \tilde{\mathbf{p}}_3\|,$$

where the rotation is eliminated and we obtain three equations in three unknowns. Since the equations only contain s^2 , we can let $c = s^2$ to reduce the degrees and eliminate the symmetries. In short, if s is a solution, then $-s$ is also a solution. However, s should be positive since it presents the relative scale of two depths. thus a solution to $c = s^2$ gives us only one geometrically feasible solution for s .

The three above mentioned equations from the vector length constraints can be solved using the Gröbner basis method [39], where the final solver performs Gauss-Jordan elimination of a 12×16 matrix and extracts up to 4 real solutions from the eigenvalues and eigenvectors of a 4×4 matrix. We denote this solver as 3PT_{svv}(GB).

Polynomial Eigenvalue Solution

To find a more efficient solution, we use the hidden variable technique [12] and choose u as the hidden variable. The problem can then be formulated as a polynomial eigenvalue problem and efficiently solved using the method of [35]. The three equations have the following form

$$\mathbf{m}_i [1, c, cv, cv^2, u, u^2]^\top = 0, \quad i = 1, 2, 3, \quad (11)$$

where \mathbf{m}_i is a 1×6 coefficient vector. We consider u as a hidden variable, then (11) can be written as

$$\mathbf{m}_i(u) [1, c, cv, cv^2]^\top = 0, \quad i = 1, 2, 3, \quad (12)$$

where $\mathbf{m}_i(u)$ is a 1×4 polynomial vector in u . We have three equations, but $[1, c, cv, cv^2]^\top$ is a 4×1 vector. To obtain a squared system, we multiply (12) with v . In this case, we have 6 equations which can be written as

$$\mathbf{M}(u) [1, c, cv, cv^2, v, cv^3]^\top = \mathbf{0}, \quad (13)$$

where $\mathbf{M}(u)$ is a 6×6 polynomial matrix in u :

$$\mathbf{M}(u) = \mathbf{M}_0 + u\mathbf{M}_1 + u^2\mathbf{M}_2, \quad (14)$$

The solutions to $1/u$ are the eigenvalues of the following matrix

$$\mathbf{A} = \begin{bmatrix} \mathbf{0} & \mathbf{I} \\ -\mathbf{M}_0^{-\top} \mathbf{M}_2^\top & -\mathbf{M}_0^{-\top} \mathbf{M}_1^\top \end{bmatrix}. \quad (15)$$

Note that there are 4 zero columns in \mathbf{M}_2 and \mathbf{M}_1 , which will result in zero eigenvalues. Based on [35], these zero columns can be removed together with the zero rows. In this case, the final solver performs the Gauss-Jordan elimination of a 6×10 matrix, and eigenvalue computations of a 4×4 matrix. We denote this polynomial eigenvalue solver as $3\text{PT}_{suv}(\text{Eigen})$.

Closed-form Solution

In addition, the system of three polynomials can be simply converted into solving a single quartic equation with a closed-form solution, which results in a much more efficient solver. Based on (11), the three monomials $\{cv^2, cv, c\}$ can be formulated as a quadratic function of u , *i.e.*, $cv^2 = g_1(u)$, $cv = g_2(u)$, $c = g_3(u)$, where g_1, g_2, g_3 are polynomials of u in degree 2. Since $(cv)^2 = (c)(cv^2)$, we have $g_2^2 = g_1 g_3$. Then we have a quartic equation in u , which can be solved in closed-form. We denote this closed-form solver as $3\text{PT}_{suv}(\text{C})$.

3.2. Inverse Depth up to Scale and Shift

In the case of inverse depths, we can use similar tricks to eliminate the rotation and translation from the original equations (7). In this case we obtain

$$\begin{aligned} \left\| \frac{s\tilde{\mathbf{q}}_1}{\beta_1 + v} - \frac{s\tilde{\mathbf{q}}_2}{\beta_2 + v} \right\| &= \left\| \frac{\tilde{\mathbf{p}}_1}{\alpha_1 + u} - \frac{\tilde{\mathbf{p}}_2}{\alpha_2 + u} \right\|, \\ \left\| \frac{s\tilde{\mathbf{q}}_1}{\beta_1 + v} - \frac{s\tilde{\mathbf{q}}_3}{\beta_3 + v} \right\| &= \left\| \frac{\tilde{\mathbf{p}}_1}{\alpha_1 + u} - \frac{\tilde{\mathbf{p}}_3}{\alpha_3 + u} \right\|, \\ \left\| \frac{s\tilde{\mathbf{q}}_2}{\beta_2 + v} - \frac{s\tilde{\mathbf{q}}_3}{\beta_3 + v} \right\| &= \left\| \frac{\tilde{\mathbf{p}}_2}{\alpha_2 + u} - \frac{\tilde{\mathbf{p}}_3}{\alpha_3 + u} \right\|. \end{aligned} \quad (16)$$

However, these equations have unknowns in the denominators, and simply multiplying the equations with the denominators results in a very complex system of equations that is difficult to solve.

To solve the equations efficiently, we first multiply (16) with $\alpha_1 + u$, and let

$$\begin{aligned} b_1 &= \frac{s(\alpha_1 + u)}{\beta_1 + v}, \quad b_2 = \frac{s(\alpha_1 + u)}{\beta_2 + v}, \quad b_3 = \frac{s(\alpha_1 + u)}{\beta_3 + v}, \\ c_2 &= \frac{\alpha_1 + u}{\alpha_2 + u}, \quad c_3 = \frac{\alpha_1 + u}{\alpha_3 + u}. \end{aligned} \quad (17)$$

Substituting (17) into (16) we have three equations

$$\begin{aligned} \|b_1\tilde{\mathbf{q}}_1 - b_2\tilde{\mathbf{q}}_2\| &= \|\tilde{\mathbf{p}}_1 - c_2\tilde{\mathbf{p}}_2\|, \\ \|b_1\tilde{\mathbf{q}}_1 - b_3\tilde{\mathbf{q}}_3\| &= \|\tilde{\mathbf{p}}_1 - c_3\tilde{\mathbf{p}}_3\|, \\ \|b_2\tilde{\mathbf{q}}_2 - b_3\tilde{\mathbf{q}}_3\| &= \|c_2\tilde{\mathbf{p}}_2 - c_3\tilde{\mathbf{p}}_3\|. \end{aligned} \quad (18)$$

In addition, by eliminating $\{s, u, v\}$ from (17) we obtain the following two equations in $\{b_1, b_2, b_3, c_2, c_3\}$

$$\begin{aligned} b_1 b_2 \beta_1 - b_1 b_3 \beta_1 - b_1 b_2 \beta_2 + b_2 b_3 \beta_2 + b_1 b_3 \beta_3 - b_2 b_3 \beta_3 &= 0, \\ c_2 c_3 \alpha_2 - c_2 c_3 \alpha_3 + c_2 \alpha_1 - c_3 \alpha_1 - c_2 \alpha_2 + c_3 \alpha_3 &= 0. \end{aligned} \quad (19)$$

Combining (19) with (18) we have 5 equations in 5 unknowns that have up to 10 real solutions. We denote this solver as $3\text{PT}_{suv}(\text{inverse})$. More details about this solver are in the appendices.

4. Focal Length Problems

In many practical scenarios, the intrinsic parameters of the cameras may not be available. However, it is often reasonable to assume that modern cameras have square-shaped pixels, and the principal point coincides with the image center [25]. This is a widely used assumption in many camera geometry solvers, where the only unknown intrinsic parameters are focal lengths, and the calibration matrices have the form $\mathbf{K}_i = \text{diag}(f_i, f_i, 1)$.

Equal and Unknown Focal Length

First, let us assume that the two cameras have unknown equal focal lengths, *i.e.*, $\mathbf{K}_1 = \mathbf{K}_2 = \text{diag}(f, f, 1)$, which is a common scenario, *e.g.*, when estimating the motion of a single uncalibrated camera. This is a 10-DOF problem w.r.t. $\{s, u, v, \mathbf{R}, \mathbf{t}, f\}$, and we need at least three 3D-3D point correspondences and one 2D-2D point correspondence, *i.e.* four 2D-2D correspondences from which three have monocular depths estimated in both images and thus can be considered as 3D-3D correspondences. Note that, here the 3D-3D point correspondences depend on the unknown focal length parameter.

In this case, we may obtain the following system of 6 equations in 6 unknowns $\{s, u, v, f, \eta_4, \lambda_4\}$

$$\begin{aligned} \|s\mathbf{K}_2^{-1}((\beta_1 + v)\mathbf{q}_1 - s(\beta_2 + v)\mathbf{q}_2)\| &= \|\mathbf{K}_1^{-1}((\alpha_1 + u)\mathbf{p}_1 - (\alpha_2 + u)\mathbf{p}_2)\|, \\ \|s\mathbf{K}_2^{-1}((\beta_1 + v)\mathbf{q}_1 - s(\beta_3 + v)\mathbf{q}_3)\| &= \|\mathbf{K}_1^{-1}((\alpha_1 + u)\mathbf{p}_1 - (\alpha_3 + u)\mathbf{p}_3)\|, \\ \|s\mathbf{K}_2^{-1}((\beta_2 + v)\mathbf{q}_2 - s(\beta_3 + v)\mathbf{q}_3)\| &= \|\mathbf{K}_1^{-1}((\alpha_2 + u)\mathbf{p}_2 - (\alpha_3 + u)\mathbf{p}_3)\|, \\ \|s\mathbf{K}_2^{-1}((\beta_1 + v)\mathbf{q}_1 - s\lambda_4\mathbf{q}_j)\| &= \|\mathbf{K}_1^{-1}((\alpha_1 + u)\mathbf{p}_1 - \eta_4\mathbf{p}_j)\|, \\ \|s\mathbf{K}_2^{-1}((\beta_2 + v)\mathbf{q}_2 - s\lambda_4\mathbf{q}_4)\| &= \|\mathbf{K}_1^{-1}((\alpha_2 + u)\mathbf{p}_2 - \eta_4\mathbf{p}_4)\|, \\ \|s\mathbf{K}_2^{-1}((\beta_3 + v)\mathbf{q}_3 - s\lambda_4\mathbf{q}_4)\| &= \|\mathbf{K}_1^{-1}((\alpha_3 + u)\mathbf{p}_3 - \eta_4\mathbf{p}_4)\|. \end{aligned}$$

To solve such a system, we need to perform Gauss-Jordan elimination of a large matrix. Moreover, the system has up to 28 real solutions. Thus, its solver is not relevant for practical applications.

To find a more efficient and practical solution, we use four 2D-2D point correspondences with their four monocular depths in both images. In this case, we obtain the following 6 equations in 4 unknowns $\{s, u, v, f\}$

$$\|s\mathbf{K}_2^{-1}((\beta_i + v)\mathbf{q}_i - s(\beta_j + v)\mathbf{q}_j)\| = \|\mathbf{K}_1^{-1}((\alpha_i + u)\mathbf{p}_i - (\alpha_j + u)\mathbf{p}_j)\|,$$

where $i, j = 1, 2, 3, 4$, $i \neq j$. In general, it is an over-constrained system. One way to solve it is to use four of these six equations in four unknowns. Such a solver only needs to perform the Gauss-Jordan elimination of a 24×32 matrix and returns up to 8 real solutions. We denote this solver as $4\text{PT}_{suv}f(\text{GB})$.

However, in this case, a smaller solver can be obtained by using all 6 polynomials. This solver performs the Gauss-Jordan elimination of a 6×8 and returns only up to 2 real solutions. We denote this solver as $4\text{PT}_{suv}f(\text{Eigen})$. Details of this solver are shown in appendices.

Different and Unknown Focal Lengths

Finally, we consider the case where $\mathbf{K}_i = \text{diag}(f_i, f_i, 1)$, $i = 1, 2$, with $f_1 \neq f_2$. This is a 11-DOF problem w.r.t. $\{s, u, v, \mathbf{R}, \mathbf{t}, f_1, f_2\}$. Thus, we need at least three 3D-3D point correspondences and one 3D-2D point correspondence, *i.e.* a correspondence where we have monocular depth only in one image. Similar to the equal and unknown focal length case, we can formulate this problem using a system of 6 equations in 6 unknowns with up to 14 real solutions. This system can be solved using a Gröbner basis method.

However, more efficient solver can be obtained using four 3D-3D point correspondences, yielding six equations in five unknowns: s, u, v, f_1, f_2 . This is an over-constrained system that can be again solved by using only five of these six equations. Such a solver performs the Gauss-Jordan elimination of a 20×24 matrix, resulting in up to four solutions, and we denote this solver as $4\text{PT}_{suv}f_{1,2}(\text{GB})$. Alternatively, by using all six equations, we can derive a significantly smaller solver with up to two real solutions. This solver performs Gauss-Jordan elimination of a 6×8 matrix, and we denote this solver as $4\text{PT}_{suv}f_{1,2}(\text{Eigen})$. Further details on the focal length solvers are provided in the appendices.

5. Experiments

We evaluated the performance of the proposed solvers, namely, the $3\text{PT}_{suv}(\text{GB})$, $3\text{PT}_{suv}(\text{Eigen})$ and $3\text{PT}_{suv}(\text{C})$ solvers for the calibrated case, the $4\text{PT}_{suv}f(\text{GB})$ and $4\text{PT}_{suv}f(\text{Eigen})$ solvers for unknown equal focal lengths, and the $4\text{PT}_{suv}f_{1,2}(\text{GB})$ and $4\text{PT}_{suv}f_{1,2}(\text{Eigen})$ solvers for varying focal lengths—on both synthetic data and real-world images. For calibrated camera pose estimation, we compared our $3\text{PT}_{suv}(\text{Eigen})$ solver to the closely related Rel3PT solver from [2], the P3P solver [15], and the

F Solver	Point Correspondence			Scale Ratio	Shift	DOF	No. of Solutions
	3D-3D	3D-2D	2D-2D				
Equal f	6-point [25]	-	-	6	-	-	6
	3p3d [16]	3	-	-	1	(0, 0)	6
	3PT ₁₀₀ f	1	2	0	1	(0, 0)	7
	3PT _{1uu} f	2	1	0	1	(u, u)	8
	3PT _{1uv} f	3	0	0	1	(u, v)	9
	3PT _{s00} f	2	1	0	s	(0, 0)	8
	3PT _{suu} f	3	0	0	s	(u, u)	9
Varying f_1, f_2	4PT _{suv} f	3	0	1	s	(u, v)	10
	7-point [26]	-	-	7	-	-	7
	4p4d [16]	4	-	-	1	(0, 0)	7
	3PT ₁₀₀ $f_{1,2}$	2	1	0	1	(0, 0)	8
	3PT _{1uu} $f_{1,2}$	3	0	0	1	(u, u)	9
	4PT _{1uu} $f_{1,2}$	3	0	1	1	(u, v)	10
	3PT _{s00} $f_{1,2}$	3	0	0	s	(0, 0)	9
$4\text{PT}_{suv}f_{1,2}$	4PT _{suv} $f_{1,2}$	3	0	1	s	(u, u)	10
	4PT _{suv} $f_{1,2}$	3	1	0	s	(u, v)	11
	4PT _{suv} $f_{1,2}$	3	1	0	s	(u, v)	14

Table 2. Different combinations of using 3D-3D, 3D-2D and 2D-2D point correspondences for focal length problems.

SPT algorithm from [46]. For the unknown equal focal length case, we compared the proposed $4\text{PT}_{suv}f(\text{GB})$ and $4\text{PT}_{suv}f(\text{Eigen})$ solvers with the 3p3d solver [16] and the 6PT solver [37]. For varying focal lengths, we compared our $4\text{PT}_{suv}f_{1,2}(\text{GB})$ and $4\text{PT}_{suv}f_{1,2}(\text{Eigen})$ solvers with the closely related 4p4d solver from [16] and the standard 7PT algorithm [26].

5.1. Computational Complexity

The complexity and run-time of a single estimation of the proposed solvers are reported in the following table.

Solver	G-J	Eigen	Poly	Time (μs)
3PT _{suv} (GB)	12×16	4×4	-	4.45
3PT _{suv} (Eigen)	6×10	4×4	-	3.42
3PT _{suv} (C)	3×6	-	4	1.46
3PT _{suv} (inverse)	54×66	12×12	-	36.9
4PT _{suv} f (GB)	24×32	8×8	-	12.5
4PT _{suv} f (Eigen)	6×8	2×2	-	2.38
4PT _{suv} $f_{1,2}$ (GB)	20×24	4×4	-	6.45
4PT _{suv} $f_{1,2}$ (Eigen)	6×8	2×2	-	2.49

5.2. Synthetic Evaluation

We generate 200 random 3D points in the cube $[-5, 5] \times [-5, 5] \times [2, 22]$ and 5,000 image pairs with random camera poses. In the case of two equal focal lengths, we set them to 500 pixels, and for the case of different focal lengths, we set them to 500 pixels and 1000 pixels. The shift of the depth is set to 10% of the average distance of the camera to the scene, and a random scale factor is also added to the depths in each camera. In the inverse depth solver, the shift is applied to the inverse depth. For the calibrated case, we compare our $3\text{PT}_{suv}(\text{GB})$, $3\text{PT}_{suv}(\text{Eigen})$, $3\text{PT}_{suv}(\text{C})$, and $3\text{PT}_{suv}(\text{inverse})$ solvers with the 5PT solver [46], the P3P algorithm [15] and the Rel3PT solver [2]. For the case of

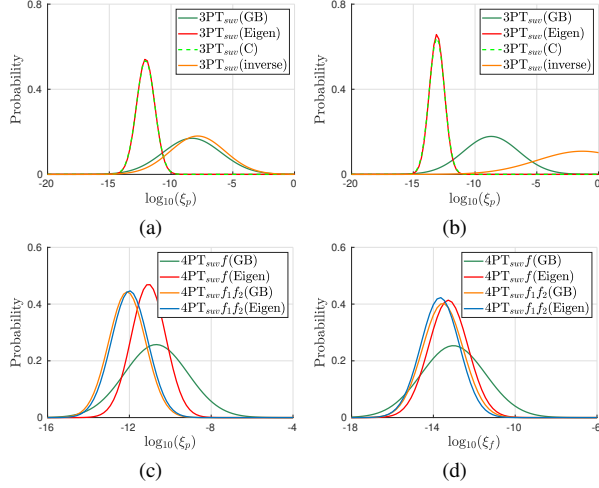


Figure 1. Numerical stability of the proposed solvers on noise-free data. **Top row:** calibrated solvers under (a) general motion, and under (b) pure rotation. **Bottom row:** (c) pose errors, and (d) focal length errors for focal length solvers.

unknown equal focal length, we compare our $4\text{PT}_{\text{suv}}f(\text{GB})$ and $4\text{PT}_{\text{suv}}f(\text{Eigen})$ solvers with the 3p3d solver [16] and the 6pt solver [37]. For two cameras with different unknown focal lengths, we compare our $4\text{PT}_{\text{suv}}f_1f_2(\text{GB})$ and $4\text{PT}_{\text{suv}}f_1f_2(\text{Eigen})$ solvers with the 4p4d solver [16] and the 7pt solver [37]. We evaluate a solver’s performance by studying the error in the estimated rotation w.r.t. the ground truth, defined as $\xi_{\mathbf{R}} = 2 \arcsin \left(\frac{\|\mathbf{R}_g - \mathbf{R}_e\|}{2\sqrt{2}} \right)$, $\xi_{\mathbf{t}} = 2 \arcsin \left(\frac{1}{2} \left\| \frac{\mathbf{t}_e}{\|\mathbf{t}_e\|} - \frac{\mathbf{t}_g}{\|\mathbf{t}_g\|} \right\| \right)$, $\xi_f = \frac{|f_e - f_g|}{f_g}$. For the different-and-unknown focal lengths problem, we evaluate the geometric mean of the focal lengths errors $\xi_f = \sqrt{\xi_{f_1}\xi_{f_2}}$. We use the \arcsin formulation for rotation [14], since the \arccos metric suffers from precision issues with noise-free data.

Numerical Stability. The top row of Fig. 1 shows the numerical stability of the proposed calibrated solvers in two configurations (left: general motion; right, pure rotation). To save space, here we show the pose error $\xi_p = \max(\xi_{\mathbf{R}}, \xi_{\mathbf{t}})$. Most of the proposed solvers are stable for all tested configurations, except for the pure rotation, where the proposed inverse depth solver cannot handle the pure rotation case. The bottom row of Fig. 1 shows the numerical stability of the proposed focal length solvers (left: \log_{10} pose errors; right, \log_{10} focal length errors). We can see that all the proposed focal length solvers are stable with noise-free data. The stability of focal length solvers under pure rotation is shown in the appendices.

Robustness to Noise. Next, we test the performance of all solvers under increasing image noise. We add Gaussian noise with standard deviation varying from 1 to 4 pixels to the image points in both cameras. Fig. 2 left column

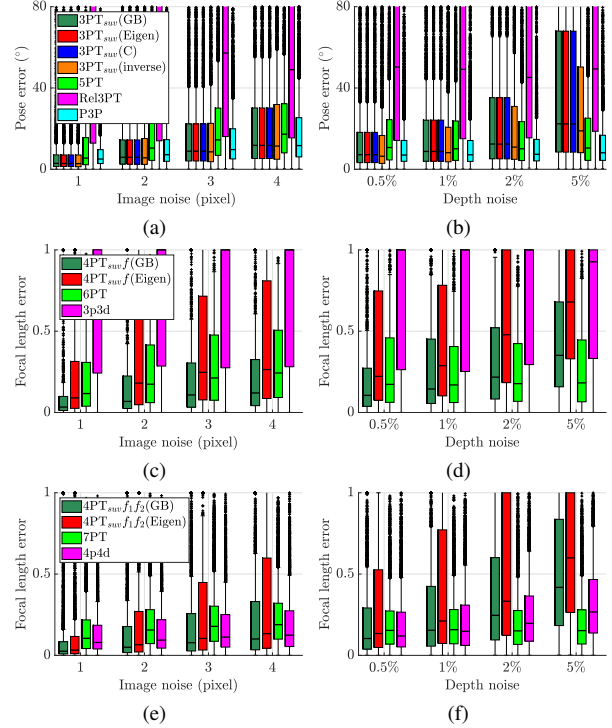


Figure 2. A comparison of the performance of the proposed solvers with SOTA under increasing (a,c,e) image noise, and (b,d,f) increasing depth noise with 2px image noise. **Top row:** Pose errors for calibrated case. **Middle row:** Focal length errors for equal and unknown focal length. **Bottom row:** Focal length errors for different and unknown focal lengths.

shows the box plot of the errors for solvers under increasing image noise (from top row to bottom row: Pose errors for calibrated case, focal length errors for equal and unknown focal length, and focal length errors for different and unknown focal lengths.). Here, we present the results as box plots, showing the 25% and 75% quartiles as boxes with a horizontal line indicating the median. Fig. 2a shows that our calibrated solvers perform well under increasing image noise. Due to the shift in the depth, the relative depth solver Rel3PT [2] does not provide accurate estimates. Since the three proposed 3PT_{suv} solvers perform similarly, we only show the results of 3PT_{suv}(Eigen) in the real experiments. Fig. 2c shows that the proposed $4\text{PT}_{\text{suv}}f(\text{GB})$ solver performs best under increasing image noise. The 3p3d solver [16], which assumes equal scale for the depth, is more sensitive to noise. Additionally, the proposed $4\text{PT}_{\text{suv}}f(\text{Eigen})$ solver, which solves a more relaxed problem, is also more sensitive to noise than the $4\text{PT}_{\text{suv}}f(\text{GB})$ solver. Fig. 2e shows the performance of different and unknown focal length solvers. In this case, the 4p4d solver [16] performs well since it can handle different scales of monocular depth. Yet, the first quartile of proposed $4\text{PT}_{\text{suv}}f_1f_2(\text{GB})$ is slightly better.

Depth	Method	Phototourism					ETH3D				
		$\epsilon_R(^{\circ}) \downarrow$	$\epsilon_t(^{\circ}) \downarrow$	mAA(R)↑	mAA(t)↑	$\tau(ms) \downarrow$	$\epsilon_R(^{\circ}) \downarrow$	$\epsilon_t(^{\circ}) \downarrow$	mAA(R)↑	mAA(t)↑	$\tau(ms) \downarrow$
-	5PT [46]	0.82	2.09	0.87	0.72	67.99	0.41	0.94	0.92	0.87	61.14
Real Depth	P3P	0.51	1.25	0.91	0.80	33.64	0.21	0.49	0.95	0.91	29.53
	Rel3PT	0.60	<u>1.40</u>	<u>0.90</u>	0.77	60.49	0.24	0.56	0.94	0.90	<u>45.86</u>
	3PT _{svu}	<u>0.59</u>	1.48	<u>0.90</u>	<u>0.78</u>	<u>52.68</u>	0.21	<u>0.54</u>	0.95	0.91	45.90
MiDAS [8]	P3P	<u>3.19</u>	<u>7.01</u>	<u>0.64</u>	<u>0.40</u>	26.62	<u>1.32</u>	<u>2.46</u>	<u>0.80</u>	<u>0.70</u>	<u>25.49</u>
	Rel3PT	4.29	10.53	0.55	0.33	<u>27.50</u>	2.83	5.85	0.65	0.48	21.70
	3PT _{svu}	1.31	3.10	0.82	0.64	44.45	0.82	1.84	0.87	0.78	37.62
DPT [50]	P3P	<u>3.35</u>	<u>7.36</u>	<u>0.63</u>	<u>0.39</u>	26.05	<u>1.38</u>	<u>2.67</u>	<u>0.79</u>	<u>0.68</u>	<u>24.77</u>
	Rel3PT	4.32	10.63	0.55	0.32	<u>26.83</u>	3.09	6.79	0.62	0.44	21.14
	3PT _{svu}	1.21	2.94	0.83	0.66	44.44	0.82	1.89	0.87	0.78	38.11
ZoeDepth [7]	P3P	1.41	3.22	0.81	0.63	<u>33.77</u>	<u>0.93</u>	<u>1.85</u>	<u>0.87</u>	<u>0.78</u>	<u>28.85</u>
	Rel3PT	3.57	8.99	0.59	0.36	27.44	1.76	3.93	0.75	0.61	28.52
	3PT _{svu}	<u>1.43</u>	<u>3.34</u>	<u>0.80</u>	<u>0.62</u>	43.45	0.88	1.85	0.87	0.78	37.98
DA V1 [61]	P3P	<u>3.08</u>	<u>6.83</u>	<u>0.65</u>	<u>0.42</u>	<u>27.69</u>	<u>1.41</u>	<u>2.81</u>	<u>0.78</u>	<u>0.68</u>	<u>24.27</u>
	Rel3PT	4.28	10.46	0.55	0.33	25.96	2.87	6.06	0.63	0.46	20.96
	3PT _{svu}	1.13	2.73	0.84	0.67	46.63	0.67	1.48	0.89	0.81	39.93
DA V2 [62]	P3P	<u>1.71</u>	<u>3.75</u>	<u>0.78</u>	<u>0.59</u>	<u>31.29</u>	<u>1.26</u>	<u>2.46</u>	<u>0.80</u>	<u>0.70</u>	<u>25.26</u>
	Rel3PT	3.84	9.62	0.57	0.35	25.33	2.96	6.47	0.63	0.45	20.47
	3PT _{svu}	1.27	2.94	0.83	0.66	45.37	0.66	1.47	0.89	0.81	39.61
Depth Pro [9]	P3P	1.27	2.98	0.82	0.65	<u>33.00</u>	0.59	1.28	0.91	0.84	<u>28.74</u>
	Rel3PT	4.13	10.90	0.55	0.32	19.07	2.43	5.75	0.69	0.52	21.95
	3PT _{svu}	<u>1.34</u>	<u>3.27</u>	<u>0.82</u>	<u>0.64</u>	43.93	<u>0.61</u>	<u>1.44</u>	<u>0.90</u>	<u>0.83</u>	38.93
UniDepth [49]	P3P	0.71	1.67	0.89	0.76	<u>34.89</u>	0.50	1.19	0.92	0.85	<u>28.84</u>
	Rel3PT	2.92	8.01	0.63	0.40	25.63	1.56	3.90	0.75	0.58	27.34
	3PT _{svu}	<u>0.74</u>	<u>1.90</u>	<u>0.89</u>	<u>0.74</u>	51.27	<u>0.59</u>	<u>1.28</u>	<u>0.91</u>	<u>0.84</u>	40.83
Metric3d V2 [27]	P3P	1.04	2.53	0.85	0.69	<u>33.37</u>	0.49	1.12	0.92	0.85	29.33
	Rel3PT	3.17	8.40	0.61	0.39	28.17	1.12	2.58	0.82	0.69	<u>32.47</u>
	3PT _{svu}	<u>1.17</u>	<u>2.91</u>	<u>0.84</u>	<u>0.66</u>	44.92	<u>0.61</u>	<u>1.31</u>	<u>0.90</u>	<u>0.84</u>	40.72
Marigold [31]	P3P	<u>1.86</u>	4.28	<u>0.75</u>	<u>0.55</u>	<u>31.01</u>	<u>1.15</u>	<u>2.34</u>	<u>0.81</u>	<u>0.70</u>	<u>26.76</u>
	Rel3PT	3.88	9.78	0.57	0.34	27.95	3.05	6.44	0.61	0.46	21.75
	3PT _{svu}	1.28	3.11	0.82	0.64	43.70	0.70	1.55	0.88	0.81	38.78
Marigold + FT [44]	P3P	<u>1.90</u>	<u>4.40</u>	<u>0.75</u>	<u>0.54</u>	<u>31.03</u>	<u>1.06</u>	<u>2.33</u>	<u>0.81</u>	<u>0.71</u>	<u>26.71</u>
	Rel3PT	3.79	9.51	0.57	0.35	27.88	3.06	6.18	0.62	0.47	21.47
	3PT _{svu}	1.26	3.03	0.82	0.65	44.40	0.66	1.57	0.89	0.81	38.25
MoGe [59]	P3P	0.78	1.88	0.89	0.75	<u>31.78</u>	0.47	1.11	0.92	0.86	<u>31.40</u>
	Rel3PT	2.98	7.94	0.64	0.40	27.30	2.27	5.05	0.69	0.51	22.71
	3PT _{svu}	<u>0.83</u>	<u>2.12</u>	<u>0.88</u>	<u>0.73</u>	54.99	<u>0.52</u>	<u>1.19</u>	<u>0.91</u>	<u>0.85</u>	41.33
Mean	P3P	<u>1.73</u>	<u>3.93</u>	<u>0.78</u>	<u>0.60</u>	<u>31.18</u>	<u>0.90</u>	<u>1.84</u>	<u>0.86</u>	<u>0.77</u>	<u>27.50</u>
	Rel3PT	3.48	8.85	0.61	0.39	29.13	2.27	4.96	0.70	0.55	25.53
	3PT _{svu}	1.13	2.74	0.84	0.67	46.69	0.65	1.45	0.90	0.82	39.83

Table 3. Rotation and translation errors (in degrees), and run-times (in milliseconds) on the Phototourism and ETH3D datasets for calibrated camera pose estimation. The **best** and the second best methods are highlighted.

We also evaluate the performance of all solvers under increasing depth noise, adding Gaussian noise to the depths with a standard deviation ranging from 0.5% to 5% of the average scene distance. To simulate real-world scenarios, we also add Gaussian noise with a standard deviation of 2 pixels to the images. In general, as shown in the right column of Fig. 2, for small depth noise, *i.e.*, 0.5% and 2%, the proposed solvers have better or comparable accuracy to the SOTA solvers. For the focal length problems, the proposed Eigenvalue solvers, which solve a more relaxed

system, are more sensitive to noise than the GB solvers. At higher noise levels, our solvers yield larger errors than point-based solvers. However, as shown in the next section, our solvers perform comparably to point-based solvers in real-world scenarios.

5.3. Real-world Experiments

Datasets. In order to test the proposed solvers on real-world data, we choose the Phototourism [29] and the ETH3D [54] datasets. The images of the Phototourism dataset

Depth	Method	Phototourism							ETH3D						
		$\epsilon_R(^{\circ}) \downarrow$	$\epsilon_t(^{\circ}) \downarrow$	$\epsilon_f \downarrow$	mAA(R)↑	mAA(t)↑	mAA(f)↑	$\tau(ms) \downarrow$	$\epsilon_R(^{\circ}) \downarrow$	$\epsilon_t(^{\circ}) \downarrow$	$\epsilon_f \downarrow$	mAA(R)↑	mAA(t)↑	mAA(f)↑	$\tau(ms) \downarrow$
Real Depth	6PT [46]	1.50	4.79	0.11	0.78	0.53	0.51	177.97	0.67	2.14	0.08	0.88	0.76	0.63	161.57
	3p3d	0.87	2.61	0.05	0.86	0.66	0.69	40.60	0.34	1.07	0.02	0.92	0.86	0.80	35.07
	4PT _{swf} f(GB)	0.89	2.69	0.06	0.86	0.67	0.68	59.21	0.30	0.94	0.01	0.94	0.88	0.89	55.27
MiDas [8]	4PT _{swf} f(Eigen)	1.28	4.16	0.09	0.81	0.56	0.57	12.71	0.34	0.99	0.01	0.93	0.86	0.88	14.52
	3p3d	9.86	28.36	0.64	0.36	0.11	0.09	28.81	4.95	12.73	0.44	0.52	0.27	0.18	25.10
	4PT _{swf} f(GB)	2.62	7.36	0.26	0.69	0.40	0.29	49.83	1.72	4.56	0.15	0.77	0.56	0.47	43.98
DPT [50]	4PT _{swf} f(Eigen)	6.70	21.76	0.38	0.45	0.15	0.16	7.43	3.95	12.19	0.24	0.57	0.30	0.30	6.69
	3p3d	9.53	27.66	0.65	0.38	0.12	0.09	30.18	5.05	13.27	0.46	0.51	0.26	0.18	25.35
	4PT _{swf} f(GB)	2.32	6.76	0.23	0.71	0.42	0.32	49.86	1.68	4.41	0.14	0.77	0.56	0.45	42.83
ZoeDepth [7]	4PT _{swf} f(Eigen)	6.14	20.62	0.36	0.48	0.17	0.17	7.59	4.17	11.45	0.23	0.57	0.30	0.31	6.57
	3p3d	6.02	19.49	0.60	0.47	0.18	0.11	36.74	2.97	8.18	0.31	0.63	0.39	0.29	27.19
	4PT _{swf} f(GB)	4.78	7.89	0.28	0.67	0.38	0.27	50.18	1.67	4.17	0.15	0.77	0.58	0.47	46.65
DA V1 [61]	4PT _{swf} f(Eigen)	6.61	21.06	0.36	0.46	0.17	0.18	7.82	3.57	9.59	0.22	0.61	0.35	0.33	7.12
	3p3d	8.92	26.21	0.66	0.39	0.13	0.09	32.87	5.22	13.87	0.42	0.50	0.27	0.18	25.53
	4PT _{swf} f(GB)	2.08	6.10	0.20	0.73	0.45	0.35	51.70	1.36	3.54	0.12	0.80	0.62	0.51	48.35
DA V2 [62]	4PT _{swf} f(Eigen)	5.12	17.21	0.31	0.53	0.21	0.20	8.42	3.10	8.76	0.21	0.63	0.35	0.31	6.97
	3p3d	6.52	20.99	0.69	0.46	0.17	0.09	36.98	4.49	12.23	0.43	0.53	0.30	0.19	28.04
	4PT _{swf} f(GB)	2.32	6.58	0.22	0.72	0.44	0.33	50.99	1.24	3.40	0.10	0.81	0.64	0.56	45.19
Depth Pro [9]	4PT _{swf} f(Eigen)	5.17	17.25	0.30	0.52	0.22	0.21	8.18	2.92	8.05	0.19	0.64	0.38	0.37	7.09
	3p3d	5.30	18.83	0.90	0.50	0.19	0.07	50.52	2.55	7.17	0.32	0.67	0.44	0.27	30.77
	4PT _{swf} f(GB)	2.63	7.69	0.26	0.69	0.41	0.30	51.83	1.12	3.21	0.10	0.83	0.67	0.58	54.32
UniDepth [49]	4PT _{swf} f(Eigen)	6.09	20.06	0.33	0.48	0.19	0.20	8.14	2.26	6.99	0.15	0.71	0.45	0.45	7.58
	3p3d	4.36	14.56	0.65	0.56	0.26	0.14	45.57	2.38	6.18	0.26	0.71	0.47	0.32	28.22
	4PT _{swf} f(GB)	1.11	3.45	0.09	0.84	0.61	0.58	57.52	0.94	2.47	0.07	0.86	0.72	0.65	50.45
Metric3d V2 [27]	4PT _{swf} f(Eigen)	1.84	6.45	0.14	0.75	0.46	0.44	11.44	1.77	5.27	0.12	0.75	0.53	0.51	8.27
	3p3d	5.37	17.08	0.61	0.51	0.21	0.12	36.79	1.97	5.85	0.21	0.71	0.49	0.39	26.35
	4PT _{swf} f(GB)	2.19	6.55	0.23	0.73	0.45	0.34	51.54	1.07	2.77	0.08	0.85	0.70	0.60	46.78
Marigold [31]	4PT _{swf} f(Eigen)	4.98	16.78	0.30	0.53	0.23	0.21	8.23	2.13	6.25	0.14	0.72	0.48	0.48	7.58
	3p3d	8.05	24.57	0.61	0.41	0.13	0.10	31.77	5.10	13.78	0.48	0.50	0.25	0.16	27.16
	4PT _{swf} f(GB)	2.41	7.00	0.25	0.70	0.42	0.30	50.88	1.28	3.39	0.12	0.80	0.63	0.50	45.67
Marigold + FT [44]	4PT _{swf} f(Eigen)	5.14	17.02	0.31	0.50	0.20	0.20	8.11	3.01	8.24	0.20	0.64	0.38	0.37	7.14
	3p3d	7.91	24.34	0.59	0.40	0.12	0.10	31.30	4.59	12.77	0.48	0.53	0.28	0.19	27.42
	4PT _{swf} f(GB)	2.32	6.59	0.23	0.71	0.43	0.32	51.49	1.17	3.32	0.12	0.82	0.65	0.55	45.12
MoGe [59]	4PT _{swf} f(Eigen)	2.22	8.22	0.17	0.71	0.42	0.39	10.05	1.69	5.19	0.11	0.76	0.54	0.54	8.06
	3p3d	6.46	20.05	0.60	0.49	0.21	0.15	36.25	3.49	9.48	0.34	0.62	0.40	0.29	27.87
	4PT _{swf} f(GB)	2.08	6.05	0.20	0.74	0.47	0.38	57.52	1.20	3.22	0.10	0.82	0.66	0.57	48.92
Mean	4PT _{swf} f(Eigen)	4.72	15.73	0.28	0.56	0.27	0.26	8.86	2.64	7.53	0.17	0.68	0.45	0.44	7.93

Table 4. Rotation and translation errors (in degrees), and run-times (in milliseconds) on the Phototourism and ETH3D datasets for the equal and unknown focal length problem. The **best** and the second best methods are highlighted.

were collected from multiple cameras obtained at different times, from different viewpoints, and with occlusions. It is a challenging dataset that is commonly used as a benchmark dataset [29] and can be used to evaluate the performance of methods in a wide range of situations. We used nine test scenes with 43,678 image pairs from this dataset, including images, ground-truth poses, and sparse depth maps. The ETH3D multi-view stereo and 3D reconstruction benchmark [54] includes a range of indoor and outdoor scenes. Ground truth geometry was acquired using a high-precision laser scanner. Images were captured with a DSLR camera and a synchronized multi-camera rig featuring cameras with varying fields of view. In total, 4,144 image pairs were used from the ETH3D dataset, and we used triangulation to get the ground truth depths.

Feature Detection and Matching. For image features, we select the popular SuperPoint (SP) features [13], widely used in SfM and localization pipelines [51]. For feature matching, we employ LightGlue (LG) [42], a state-of-the-

art deep learning-based method that demonstrates significant improvements over traditional matching methods.

Monocular Depth Estimation. We used 11 different monocular depth estimation methods to obtain the depth data, including MiDas [8], DPT [50], ZoeDepth [7], DA V1 (Depth Anything V1) [61], DA V2 (Depth Anything V2) [62], Depth Pro [9], UniDepth [49], Metric 3d V2 [27], Marigold [31], Marigold +FT (Fine tuning) [44], and MoGe [59]. While using depth maps does not add computational overhead, incorporating learning-based methods does introduce additional costs. However, in some applications, depth estimation methods serve multiple tasks, so this computational cost is not solely attributable to the pose estimation method.

Experimental Results. Our solvers are integrated into GC-RANSAC [4] and PoseLib [38] for robust estimation. To evaluate the performance of the minimal solvers, we first test all solvers within GC-RANSAC with local optimization

turned off and fixed 1000 iterations.

(i) *Calibrated camera pose estimation.* Table 3 shows the rotation and translation errors (in degrees), and run-times (in milliseconds) on the Phototourism and ETH3D datasets for calibrated camera pose estimation. Both the Phototourism and ETH3D datasets contain image pairs where all the solvers fail to find reasonable results. Thus for each dataset, we first calculate the median of the rotation and translation errors for each scene, and then report the mean over all the scenes. In addition, we also report the mAA (mean average accuracy) [28] of the rotation and translation errors under 10 degrees. With the scale and shift formulation, our solver gives more stable results for different monocular depths. With very accurate depth, the P3P algorithm performs slightly better, but the P3P algorithm is more sensitive to noise in the depth data. Our solver and the P3P solver using depth from [49, 59] perform slightly better than the 5PT algorithm on Phototourism. Here, we skip the inverse depth solver 3PT_{suv}(inverse) since it is slower and does not give better results than the 3PT_{suv} solver. Results for 3PT_{suv}(inverse) are shown in the appendices.

(ii) *Equal and unknown focal length problem.* Table 4 shows the rotation and translation errors (in degrees), focal length errors, and run-times (in milliseconds) on the Phototourism and ETH3D datasets for two cameras with equal and unknown focal length. Since the focal length of both cameras is unknown, we can not apply the P4P_f algorithm as the focal length is required to obtain 3D points from 2D points and corresponding depth values. Compared to the relative depth 3p3d solver [16], the proposed 4PT_{suv}_f(GB) solver is more stable and more robust to the quality of the depth data, as evident from the fact that it outperforms 3p3d for all depth predictors. Due to space limitation, results for two cameras with varying focal lengths, and results with Poselib are shown in the appendices.

Limitations. Compared to standard point-based focal length solvers, the proposed solvers encounter fewer degenerate cases. The formulation allows us to handle pure rotation effectively. However, there are still several degenerate cases similar to those in point-based solvers; for example, four coplanar points and cases of pure translation can introduce degeneracies in focal length recovery [30].

6. Conclusion

This paper addresses the problem of estimating the relative pose between two cameras using monocular depth predictions for both images. Unlike prior work, which only took the unknown scale factors of the depth maps into account, this paper models the fact that the depth maps are defined up to unknown scale and shift parameters. We propose multiple solvers that jointly estimate scale, shift, and relative pose. We consider three cases: (1) two calibrated cameras, (2) two uncalibrated cameras with a shared focal length, (3)

two uncalibrated cameras with different focal lengths. Efficient solvers are proposed for all three cases and experiments on real and synthetic data show the practical relevance of our solvers. In particular, we evaluate our novel solvers on two real-world datasets and 11 depth prediction networks, showing that our solvers achieve state-of-the-art results.

Acknowledgements Y. D., V.V. and Z.K. were supported by the Czech Science Foundation (GAČR) JUNIOR STAR Grant (No. 22-23183M). V. K. was supported by the project no. 1/0373/23. and the TERAIS project, a Horizon-Widera-2021 program of the European Union under the Grant agreement number 101079338. T. S. was supported by the EU Horizon 2020 project RICAIP (grant agreement No. 857306).

Appendices

This appendix provides the following information: Sec. A provides more details about the solvers, including general solutions to the problems using 3 point correspondences and details about the 3PT_{suv}(inverse) and 4PT focal length solvers. Sec. B provides more experimental results, including stability for focal length solvers under pure rotation, discussion on the 3PT_{suv}(inverse) solver, and more results from GC-RANSAC and Poselib.

A. More Details about the Solvers

A.1. Solvers Using Three Point Correspondences

For calibrated camera pose estimation with monocular depth, all possible cases can be addressed using three point correspondences and a varying number of monocular depth estimates. Similarly, for focal length problems, most can be solved using three point correspondences and a varying number of depth estimates. In general, any problem involving three point correspondences can be solved using a similar approach. Here we show the solution to the 3PT_{s00} case, *i.e.*, the shifts in the monocular depths are omitted and we only consider the scale. The minimal case is one 3D-3D point correspondence with two 3D-2D point correspondences. We have

$$s\beta_1\tilde{\mathbf{q}}_1 = \alpha_1\mathbf{R}\tilde{\mathbf{p}}_1 + \mathbf{t}, \quad (20)$$

$$s\beta_2\tilde{\mathbf{q}}_2 = \eta_2\mathbf{R}\tilde{\mathbf{p}}_2 + \mathbf{t}, \quad (21)$$

$$s\beta_3\tilde{\mathbf{q}}_3 = \eta_3\mathbf{R}\tilde{\mathbf{p}}_3 + \mathbf{t}, \quad (22)$$

where $\alpha_1, \beta_1, \beta_2, \beta_3$ are known from the monocular depths, and η_2, η_3 are unknown depths. We can obtain three equations in three unknowns from the differences (20)-(21), (20)-(22), (21)-(22):

$$\|s\beta_1\tilde{\mathbf{q}}_1 - s\beta_2\tilde{\mathbf{q}}_2\| = \|\alpha_1\tilde{\mathbf{p}}_1 - \eta_2\tilde{\mathbf{p}}_2\|, \quad (23)$$

$$\|s\beta_1\tilde{\mathbf{q}}_1 - s\beta_3\tilde{\mathbf{q}}_3\| = \|\alpha_1\tilde{\mathbf{p}}_1 - \eta_3\tilde{\mathbf{p}}_3\|, \quad (23)$$

$$\|s\beta_2\tilde{\mathbf{q}}_2 - s\beta_3\tilde{\mathbf{q}}_3\| = \|\eta_2\tilde{\mathbf{p}}_2 - \eta_3\tilde{\mathbf{p}}_3\|.$$

The system of equations (23) can be solved similarly as for the 3PT_{suv} solver presented in Sec.3.1 of the main paper. In general, all the problems using three point correspondences can be converted into solving three equations in three unknowns. They differ in the number of depth parameters for the 2D points.

A.2. Details for the 3PT_{suv}(inverse) Solver

To find the constraints on b_1, b_2, b_3, c_2, c_3 (see Eq(14) in the main paper), We first create an ideal J generated by these 5 polynomials (see Eq(12) in the main paper). Then, the unknown parameters s, u, v are eliminated from the generators of J by computing the generators of the elimination ideal $J_1 = J \cap \mathbb{C}[\alpha_1, \alpha_2, \dots, c_2, c_3]$. These generators can be computed using the following Macaulay2 [23] code

```
R = QQ[s, u, v, α1, α2, α3, β1, β2, β3, b1, b2, b3, c2, c3];
eq = {b1(β1 + v) - s(α1 + u), b2(β2 + v) - s(α1 + u),
      b3(β3 + v) - s(α1 + u), c2(α2 + u) - (α1 + u),
      c3(α3 + u) - (α1 + u)};
J = ideal(eq);
J1 = eliminate(J, {s, u, v});
g = mingens J1;
"eq14.txt" << toString g << close;
```

In this case, we have 5 quadratic polynomials in 5 unknowns, which can be solved using the GB method [12]. Based on [39], we obtain an elimination template of size 54×66 and there are 12 solutions. Note that there are two trivial solutions $b_2 = b_3 = c_2 = c_3 = 0, \|b_1\tilde{q}_1\| = \|\tilde{p}_1\|$, which should be eliminated. Hence, there are up to 10 possible solutions. However, this 3PT_{suv}(inverse) solver is much more complex than the 3PT_{suv} solvers, and in the next section, we show that this solver does not give better results with affine invariant inverse depth.

A.3. Details for 4PT(Eigen) Solvers

4PT_{suv}f(Eigen). Here we provide more details on the 4PT_{suv}f(Eigen) solver presented in Sec. 4 paragraph "Equal and Unknown Focal Length" of the main paper.

In this case, by using four 3D-3D point correspondences, we can rewrite the six equations for this problem (L289 of the main paper) as

$$\mathbf{m}_i [1, c, cv, cv^2, u, u^2, f^2, cf^2]^\top = 0, i = 1, 2, \dots, 6, \quad (24)$$

where \mathbf{m}_i is a 1×8 coefficient matrix. Since these equations only contain f^2 , we let $w = f^2$ and consider w as the hidden variable. Then (24) can be written as

$$\mathbf{M}(w) [1, c, cv, cv^2, u, u^2]^\top = 0, \quad (25)$$

where $\mathbf{M}(w)$ is a 6×6 polynomial matrix in w . It can be solved similar to Sec. 3.1, and there are only two possible solutions.

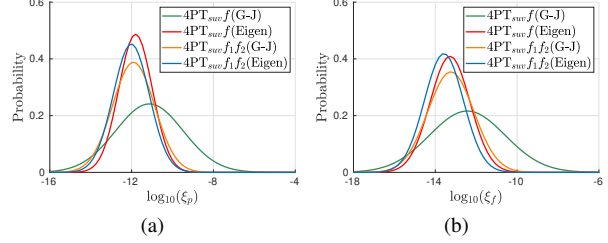


Figure 3. Numerical stability of the focal length solvers under pure rotation. We report (a) the rotation error, and (b) the focal length error.

4PT_{suv}f_{1,2}(Eigen). For this problem, we have the following six equations

$$\mathbf{m}_i [1, c, cf_2^2, cf_2^2v, cf_2^2v^2, f_1^2, f_1^2u, f_1^2u^2]^\top = 0, \quad (26)$$

where $i = 1, 2, \dots, 6$. We consider v as a hidden variable, and (26) can be written as

$$\mathbf{M}(v) [1, c, cf_2^2, f_1^2, f_1^2u, f_1^2u^2]^\top = 0, \quad (27)$$

where $\mathbf{M}(v)$ is a 6×6 polynomial matrix in v . It can be solved similar to Sec. 3.1, and there are only two possible solutions.

B. More Experiments

B.1. Stability Under Pure Rotation

Figure 3 evaluates the numerical stability of the focal length solvers in the case of a pure rotation between the two cameras. By construction, the focal length solvers can handle pure rotation since we first eliminate the translation, *i.e.*, the constraints used to solve the problems are independent of translation. This can also be seen from the results of the experiment. Note that if we have prior knowledge of the motion, *i.e.*, if we know that the cameras are undergoing pure rotation, then fewer point correspondences can be used to solve all the problems.

B.2. Results for 3PT_{suv}(inverse)

This solver was derived to be used with affine invariant inverse depths, *e.g.*, obtained via Depth Anything [61]. However, we find that the 3PT_{suv}(inverse) solver does not improve the accuracy even for affine invariant inverse depths. In addition, 3PT_{suv}(inverse) is much more time-consuming than 3PT_{suv}(GB) and 3PT_{suv}(Eigen) solvers as shown in Table 5. As such, we did not evaluate the 3PT_{suv}(inverse) solver in the main paper.

B.3. Results for Varying Focal Lengths From GC-RANSAC

Table 6 presents the results for the problem of different and unknown focal lengths using GC-RANSAC. The proposed

Depth	Method	Phototourism				
		$\epsilon_R(^{\circ}) \downarrow$	$\epsilon_t(^{\circ}) \downarrow$	mAA(R)↑	mAA(t)↑	$\tau(ms) \downarrow$
DA V2 [62]	3PT _{suv}	1.27	2.94	0.83	0.66	45.37
	3PT _{suv} (inverse)	1.28	3.02	0.83	0.65	194.77

Table 5. Comparison between 3PT_{suv} and 3PT_{suv}(inverse) with Depth anything V2 [62] on the Phototourism dataset.

4PT_{suv} $f_{1,2}$ (GB) solver, which accounts for both scale and shift in monocular depth, outperforms the state-of-the-art 4p4d solver [16] that considers only the scale effect. With a good depth prior, the 4PT_{suv} $f_{1,2}$ (GB) solver also outperforms the standard 7PT algorithm. The 4PT_{suv} $f_{1,2}$ (Eigen) solver is very fast but sensitive to noise, which is consistent to our synthetic evaluation.

B.4. PoseLib Results

In Table 7, we present results equivalent to Table 3 in the main paper, but for solvers implemented into the PoseLib [38] framework. The PoseLib implementation uses LO-RANSAC [11], with local optimization (LO) refining the pose estimates by minimizing the Sampson error using the Levenberg-Marquardt method. We use the same setup (fixed 1000 RANSAC iterations, 1px epipolar threshold) and evaluation metrics as for Table 3 in the main paper. The runtimes are reported on an Intel Icelake 6338 2GHz processor. The results are consistent with those presented in the main paper.

References

- [1] K Somani Arun, Thomas S Huang, and Steven D Blostein. Least-squares fitting of two 3-d point sets. *IEEE Transactions on pattern analysis and machine intelligence*, 1987. 1
- [2] Jonathan Astermank, Yaqing Ding, Viktor Larsson, and Anders Heyden. Fast relative pose estimation using relative depth. In *International Conference on 3D Vision (3DV)*, 2024. 2, 3, 5, 6
- [3] Daniel Barath and Zuzana Kukelova. Relative pose from sift features. In *European Conference on Computer Vision*, pages 454–469. Springer, 2022. 2
- [4] Daniel Barath and Jiří Matas. Graph-cut RANSAC. In *Computer Vision and Pattern Recognition (CVPR)*, 2018. 8, 12
- [5] Daniel Barath, Tekla Toth, and Levente Hajder. A minimal solution for two-view focal-length estimation using two affine correspondences. In *Proceedings of the IEEE Conference on Computer Vision and Pattern Recognition*, 2017. 2
- [6] Jacob Bentolila and Joseph M Francos. Conic epipolar constraints from affine correspondences. *Computer Vision and Image Understanding*, 2014. 2
- [7] Shariq Farooq Bhat, Reiner Birk, Diana Wofk, Peter Wonka, and Matthias Müller. Zoedepth: Zero-shot transfer by combining relative and metric depth. *arXiv preprint arXiv:2302.12288*, 2023. 7, 8, 12, 13
- [8] Reiner Birk, Diana Wofk, and Matthias Müller. Midas v3. 1-a model zoo for robust monocular relative depth estimation. *arXiv preprint arXiv:2307.14460*, 2023. 7, 8, 12, 13
- [9] Aleksei Bochkovskii, Amaël Delaunoy, Hugo Germain, Marcel Santos, Yichao Zhou, Stephan R Richter, and Vladlen Koltun. Depth pro: Sharp monocular metric depth in less than a second. *arXiv preprint arXiv:2410.02073*, 2024. 2, 7, 8, 12, 13
- [10] Martin Bujnak, Zuzana Kukelova, and Tomas Pajdla. A general solution to the p4p problem for camera with unknown focal length. In *2008 IEEE Conference on Computer Vision and Pattern Recognition*. IEEE, 2008. 1
- [11] Ondřej Chum, Jiří Matas, and Josef Kittler. Locally optimized ransac. In *Pattern Recognition: 25th DAGM Symposium, Magdeburg, Germany, September 10-12, 2003. Proceedings 25*, pages 236–243. Springer, 2003. 11
- [12] David A Cox, John Little, and Donal O’shea. *Using algebraic geometry*. Springer Science & Business Media, 2006. 3, 10
- [13] Daniel DeTone, Tomasz Malisiewicz, and Andrew Rabinovich. Superpoint: Self-supervised interest point detection and description. In *Proceedings of the IEEE conference on computer vision and pattern recognition workshops*, 2018. 8
- [14] Yaqing Ding, Chiang-Heng Chien, Viktor Larsson, Karl Åström, and Benjamin Kimia. Minimal solutions to generalized three-view relative pose problem. In *International Conference on Computer Vision (ICCV)*, 2023. 6
- [15] Yaqing Ding, Jian Yang, Viktor Larsson, Carl Olsson, and Kalle Åström. Revisiting the p3p problem. In *Computer Vision and Pattern Recognition (CVPR)*, 2023. 1, 3, 5
- [16] Yaqing Ding, Václav Vávra, Snehal Bhayani, Qianliang Wu, Jian Yang, and Zuzana Kukelova. Fundamental matrix estimation using relative depths. In *European Conference on Computer Vision (ECCV)*, 2024. 2, 5, 6, 9, 11, 12
- [17] Ivan Eichhardt and Daniel Barath. Relative pose from deep learned depth and a single affine correspondence. In *European Conference on Computer Vision (ECCV)*, 2020. 2
- [18] Martin A Fischler and Robert C Bolles. Random sample consensus: a paradigm for model fitting with applications to image analysis and automated cartography. *Communications of the ACM*, 1981. 2
- [19] Friedrich Fraundorfer, Petri Tanskanen, and Marc Pollefeys. A minimal case solution to the calibrated relative pose problem for the case of two known orientation angles. In *European Conference on Computer Vision (ECCV)*, 2010. 2
- [20] Xiao-Shan Gao, Xiao-Rong Hou, Jianliang Tang, and Hang-Fei Cheng. Complete solution classification for the perspective-three-point problem. *IEEE transactions on pattern analysis and machine intelligence*, 2003. 1
- [21] Clément Godard, Oisin Mac Aodha, Michael Firman, and Gabriel J Brostow. Digging into self-supervised monocular depth estimation. In *International Conference on Computer Vision (ICCV)*, 2019. 2
- [22] Herbert Goldstein, Charles Poole, John Safko, and Stephen R Addison. Classical mechanics. *American Association of Physics Teachers*, 2002. 1

Depth	Method	Phototourism							ETH3D						
		$\epsilon_R(^{\circ}) \downarrow$	$\epsilon_t(^{\circ}) \downarrow$	$\epsilon_f \downarrow$	mAA(R)↑	mAA(t)↑	mAA(f)↑	$\tau(ms) \downarrow$	$\epsilon_R(^{\circ}) \downarrow$	$\epsilon_t(^{\circ}) \downarrow$	$\epsilon_f \downarrow$	mAA(R)↑	mAA(t)↑	mAA(f)↑	$\tau(ms) \downarrow$
-	7PT [26]	6.33	14.61	0.25	0.46	0.25	0.24	39.62	4.03	5.74	0.22	0.57	0.49	0.37	35.20
Real Depth	4p4d [16]	3.59	8.00	0.18	0.61	0.39	0.37	15.78	1.62	1.91	0.09	0.72	0.73	0.58	14.14
	4PT _{svf} _{1,2} (GB)	2.47	6.97	0.14	0.69	0.42	0.44	59.88	1.22	2.05	0.07	0.77	0.74	0.63	56.87
	4PT _{svf} _{1,2} (Eigen)	2.93	8.22	<u>0.16</u>	<u>0.65</u>	<u>0.39</u>	<u>0.40</u>	11.74	1.38	2.31	<u>0.08</u>	<u>0.76</u>	<u>0.73</u>	<u>0.61</u>	<u>14.59</u>
MiDAS [8]	4p4d	13.49	38.24	<u>0.37</u>	0.21	0.06	0.12	<u>14.84</u>	9.61	21.07	0.47	0.32	0.16	0.14	<u>12.67</u>
	4PT _{svf} _{1,2} (GB)	6.85	20.28	0.29	0.43	0.16	0.19	53.66	5.61	14.13	0.24	0.47	0.27	0.30	48.14
	4PT _{svf} _{1,2} (Eigen)	9.33	28.08	<u>0.37</u>	<u>0.32</u>	<u>0.11</u>	<u>0.13</u>	6.82	7.86	<u>17.75</u>	<u>0.31</u>	<u>0.38</u>	<u>0.21</u>	<u>0.19</u>	6.29
DPT [50]	4p4d	13.11	36.42	<u>0.36</u>	0.22	0.07	0.12	<u>14.49</u>	10.21	25.02	0.49	0.30	0.14	0.12	<u>12.63</u>
	4PT _{svf} _{1,2} (GB)	6.18	19.17	0.28	0.45	0.18	0.21	53.76	5.30	14.09	0.23	0.49	0.28	0.29	49.55
	4PT _{svf} _{1,2} (Eigen)	8.57	26.71	<u>0.36</u>	<u>0.35</u>	<u>0.12</u>	<u>0.14</u>	6.96	7.68	<u>17.26</u>	<u>0.32</u>	<u>0.39</u>	<u>0.20</u>	<u>0.22</u>	6.06
ZoeDepth [7]	4p4d	9.41	25.64	<u>0.32</u>	0.32	<u>0.12</u>	<u>0.16</u>	15.72	6.92	12.70	0.35	<u>0.42</u>	<u>0.29</u>	0.21	<u>13.53</u>
	4PT _{svf} _{1,2} (GB)	7.05	19.41	0.29	0.42	0.17	0.19	54.01	5.10	11.99	0.22	0.50	0.31	0.32	49.16
	4PT _{svf} _{1,2} (Eigen)	9.56	<u>25.54</u>	0.34	<u>0.33</u>	<u>0.12</u>	0.15	7.37	6.84	15.73	<u>0.31</u>	<u>0.42</u>	0.24	<u>0.22</u>	6.82
DA V1 [61]	4p4d	12.34	34.73	0.35	0.25	0.08	0.13	15.09	10.24	23.57	0.51	0.31	0.16	0.13	<u>12.67</u>
	4PT _{svf} _{1,2} (GB)	5.46	17.00	0.26	0.49	0.21	0.23	54.91	4.28	11.01	0.19	0.53	0.32	0.35	49.45
	4PT _{svf} _{1,2} (Eigen)	7.33	23.41	<u>0.33</u>	<u>0.39</u>	<u>0.14</u>	<u>0.16</u>	7.74	6.15	<u>14.94</u>	<u>0.28</u>	<u>0.44</u>	<u>0.23</u>	<u>0.25</u>	6.75
DA V2 [62]	4p4d	9.64	27.69	0.34	0.31	0.11	0.15	<u>15.45</u>	9.35	20.00	0.45	0.33	0.18	0.12	<u>13.07</u>
	4PT _{svf} _{1,2} (GB)	5.78	17.37	0.26	0.48	0.20	0.23	54.27	3.98	10.23	0.20	0.55	0.33	0.35	48.34
	4PT _{svf} _{1,2} (Eigen)	7.65	23.42	<u>0.32</u>	<u>0.39</u>	<u>0.15</u>	<u>0.18</u>	7.92	6.37	<u>14.28</u>	<u>0.28</u>	<u>0.44</u>	<u>0.25</u>	<u>0.25</u>	6.92
Depth Pro [9]	4p4d	8.70	<u>23.50</u>	<u>0.31</u>	<u>0.35</u>	<u>0.14</u>	<u>0.17</u>	<u>15.41</u>	5.73	<u>10.11</u>	0.31	0.48	<u>0.32</u>	0.25	<u>13.70</u>
	4PT _{svf} _{1,2} (GB)	6.63	18.70	0.28	0.44	0.19	0.20	53.93	3.71	8.84	0.17	0.59	0.39	0.41	49.18
	4PT _{svf} _{1,2} (Eigen)	8.92	25.25	0.34	<u>0.35</u>	<u>0.14</u>	0.16	7.47	4.86	11.41	<u>0.23</u>	<u>0.51</u>	<u>0.32</u>	<u>0.32</u>	7.50
UniDepth [49]	4p4d	4.84	12.36	0.22	0.53	0.27	0.29	<u>16.58</u>	4.80	8.42	0.27	0.51	0.39	0.28	<u>13.83</u>
	4PT _{svf} _{1,2} (GB)	2.97	9.08	0.17	0.64	0.36	0.38	58.73	2.95	7.42	0.15	0.62	0.46	0.45	51.26
	4PT _{svf} _{1,2} (Eigen)	3.65	11.41	<u>0.20</u>	<u>0.59</u>	<u>0.31</u>	<u>0.32</u>	11.28	4.35	9.68	<u>0.19</u>	<u>0.54</u>	0.37	<u>0.37</u>	7.85
Metric3d V2 [27]	4p4d	8.04	21.41	0.30	0.37	<u>0.16</u>	<u>0.18</u>	15.64	5.14	9.23	0.29	0.48	0.36	0.28	<u>13.64</u>
	4PT _{svf} _{1,2} (GB)	5.61	16.47	0.25	0.48	0.21	0.23	54.24	3.32	8.28	0.17	0.61	0.42	0.42	48.91
	4PT _{svf} _{1,2} (Eigen)	7.73	21.98	0.32	<u>0.39</u>	<u>0.16</u>	<u>0.18</u>	7.55	4.53	10.87	<u>0.22</u>	<u>0.54</u>	0.34	<u>0.35</u>	7.39
Marigold [31]	4p4d	12.23	35.36	0.35	0.25	0.08	0.13	<u>14.64</u>	9.33	24.99	0.49	0.32	0.15	0.13	<u>12.87</u>
	4PT _{svf} _{1,2} (GB)	6.06	17.47	0.27	0.46	0.19	0.21	54.12	4.21	10.06	0.20	0.55	0.34	0.34	50.12
	4PT _{svf} _{1,2} (Eigen)	8.29	23.59	<u>0.33</u>	<u>0.36</u>	<u>0.14</u>	<u>0.16</u>	7.43	5.71	<u>12.91</u>	<u>0.26</u>	<u>0.47</u>	<u>0.28</u>	<u>0.28</u>	6.61
Marigold + FT [44]	4p4d	12.28	35.61	0.35	0.25	0.07	0.13	<u>14.89</u>	9.82	23.44	0.46	0.32	0.17	0.13	<u>12.85</u>
	4PT _{svf} _{1,2} (GB)	5.78	16.67	0.26	0.47	0.20	0.22	53.93	3.83	9.11	0.19	0.56	0.37	0.36	48.65
	4PT _{svf} _{1,2} (Eigen)	7.83	22.21	<u>0.32</u>	<u>0.38</u>	<u>0.15</u>	<u>0.17</u>	7.54	5.13	<u>12.48</u>	<u>0.25</u>	<u>0.49</u>	<u>0.30</u>	<u>0.29</u>	7.15
MoGe [59]	4p4d	5.28	14.00	0.24	0.50	0.25	0.27	<u>16.14</u>	4.65	7.86	0.26	0.52	0.40	0.29	<u>13.85</u>
	4PT _{svf} _{1,2} (GB)	3.34	10.18	0.18	0.62	0.34	0.36	66.46	3.00	6.48	0.16	0.63	0.46	0.45	51.13
	4PT _{svf} _{1,2} (Eigen)	4.31	13.26	<u>0.23</u>	<u>0.55</u>	<u>0.28</u>	<u>0.30</u>	13.54	4.08	9.18	<u>0.19</u>	<u>0.56</u>	0.38	<u>0.38</u>	8.43
Mean	4p4d	9.41	26.08	0.31	0.35	0.15	0.18	<u>15.39</u>	7.29	15.69	0.37	0.42	0.29	0.22	<u>13.29</u>
	4PT _{svf} _{1,2} (GB)	5.35	15.73	0.25	0.50	0.24	0.26	55.99	3.87	9.48	0.18	0.57	0.39	0.39	50.06
	4PT _{svf} _{1,2} (Eigen)	7.17	21.09	0.30	<u>0.42</u>	<u>0.18</u>	<u>0.20</u>	8.61	5.41	<u>12.40</u>	<u>0.24</u>	<u>0.49</u>	<u>0.32</u>	<u>0.31</u>	7.70

Table 6. Rotation and translation errors (in degrees), and run-times (in milliseconds) on the Phototourism and ETH3D datasets for the varying focal lengths problem with GC-RANSAC [4]. The **best** and the second best methods are highlighted.

[23] Daniel R. Grayson and Michael E. Stillman. Macaulay2, a software system for research in algebraic geometry. Available at <http://www2.macaulay2.com>, 1992. **10**

[24] Banglei Guan and Ji Zhao. Relative pose estimation for multi-camera systems from point correspondences with scale ratio. In *Proceedings of the 30th ACM International Conference on Multimedia*, 2022. **2**

[25] Richard Hartley and Hongdong Li. An efficient hidden variable approach to minimal-case camera motion estimation. *Trans. Pattern Analysis and Machine Intelligence (PAMI)*, 2012. **1**, **4**, **5**

[26] Richard Hartley and Andrew Zisserman. *Multiple view geometry in computer vision*. Cambridge university press, 2003. **1**, **5**, **12**

[27] Mu Hu, Wei Yin, Chi Zhang, Zhipeng Cai, Xiaoxiao Long, Hao Chen, Kaixuan Wang, Gang Yu, Chunhua Shen, and Shaojie Shen. Metric3d v2: A versatile monocular geometric foundation model for zero-shot metric depth and surface normal estimation. *arXiv preprint arXiv:2404.15506*, 2024. **2**, **7**, **8**, **12**, **13**

[28] Yuhe Jin, Dmytro Mishkin, Anastasiia Mishchuk, Jiri Matas, Pascal Fua, Kwang Moo Yi, and Eduard Trulls. Image matching across wide baselines: From paper to practice. *International Journal of Computer Vision (IJCV)*, 2020. **9**

[29] Yuhe Jin, Dmytro Mishkin, Anastasiia Mishchuk, Jiri Matas, Pascal Fua, Kwang Moo Yi, and Eduard Trulls. Image Matching across Wide Baselines: From Paper to Practice. *International Journal of Computer Vision*, 2020. **7**, **8**

[30] Fredrik Kahl and Bill Triggs. Critical motions in euclidean structure from motion. In *Computer Vision and Pattern Recognition (CVPR)*, 1999. **9**

[31] Bingxin Ke, Anton Obukhov, Shengyu Huang, Nando Metzger, Rodrigo Caye Daudt, and Konrad Schindler. Repurposing diffusion-based image generators for monocular depth estimation. In *Proceedings of the IEEE/CVF Conference on Computer Vision and Pattern Recognition (CVPR)*, 2024. **2**, **7**, **8**, **12**, **13**

[32] Tong Ke and Stergios I Roumeliotis. An efficient algebraic solution to the perspective-three-point problem. In *Proceedings of the IEEE Conference on Computer Vision and Pattern Recognition*, pages 7225–7233, 2017. **1**

[33] Laurent Kneip, Davide Scaramuzza, and Roland Siegwart. A novel parametrization of the perspective-three-point problem for a direct computation of absolute camera position and

Depth	Method	Phototourism					ETH3D				
		$\epsilon_R(^{\circ}) \downarrow$	$\epsilon_t(^{\circ}) \downarrow$	mAA(R)↑	mAA(t)↑	$\tau(ms) \downarrow$	$\epsilon_R(^{\circ}) \downarrow$	$\epsilon_t(^{\circ}) \downarrow$	mAA(R)↑	mAA(t)↑	$\tau(ms) \downarrow$
-	5PT	0.70	1.92	0.88	0.73	36.78	0.36	0.84	0.92	0.87	35.47
Real Depth	P3P	0.65	1.76	0.90	0.75	20.53	0.31	0.70	0.94	0.90	21.78
	Rel3PT	0.67	1.82	0.89	0.74	73.71	0.37	0.82	0.92	0.88	67.84
	3PT _{svu}	<u>0.66</u>	<u>1.80</u>	<u>0.90</u>	<u>0.75</u>	<u>29.51</u>	<u>0.33</u>	<u>0.72</u>	<u>0.93</u>	<u>0.89</u>	<u>32.88</u>
MiDAS [8]	P3P	<u>0.89</u>	<u>2.52</u>	<u>0.80</u>	<u>0.64</u>	15.98	<u>0.48</u>	<u>1.11</u>	<u>0.87</u>	<u>0.81</u>	16.83
	Rel3PT	5.93	10.69	0.59	0.43	<u>23.88</u>	5.11	4.28	0.66	0.58	<u>25.68</u>
	3PT _{svu}	0.72	1.99	0.88	0.72	25.15	0.41	1.02	0.90	0.84	26.96
DPT [50]	P3P	<u>0.90</u>	<u>2.60</u>	<u>0.80</u>	<u>0.63</u>	14.49	<u>0.45</u>	<u>1.14</u>	<u>0.87</u>	<u>0.81</u>	15.66
	Rel3PT	6.55	12.18	0.56	0.40	<u>23.59</u>	4.74	4.71	0.64	0.56	<u>25.68</u>
	3PT _{svu}	0.71	1.99	0.88	0.73	25.47	0.42	1.06	0.90	0.84	26.57
ZoeDepth [7]	P3P	0.71	1.93	0.88	0.73	16.88	<u>0.46</u>	<u>1.03</u>	0.90	0.84	17.46
	Rel3PT	7.75	15.71	0.49	0.36	25.70	2.23	2.61	0.76	0.70	35.42
	3PT _{svu}	<u>0.72</u>	<u>2.00</u>	<u>0.88</u>	<u>0.72</u>	<u>24.65</u>	0.43	1.03	<u>0.89</u>	<u>0.83</u>	<u>26.61</u>
DA V1 [61]	P3P	<u>0.82</u>	<u>2.37</u>	<u>0.82</u>	<u>0.66</u>	15.16	<u>0.44</u>	<u>1.05</u>	<u>0.86</u>	<u>0.80</u>	15.91
	Rel3PT	5.94	12.71	0.55	0.38	<u>23.47</u>	4.39	4.88	0.64	0.56	<u>25.81</u>
	3PT _{svu}	0.70	1.95	0.88	0.73	26.55	0.41	0.94	0.91	0.85	27.31
DA V2 [62]	P3P	<u>0.73</u>	<u>1.99</u>	<u>0.87</u>	<u>0.71</u>	16.20	<u>0.42</u>	<u>1.05</u>	<u>0.87</u>	<u>0.81</u>	16.45
	Rel3PT	5.42	12.72	0.54	0.37	<u>23.37</u>	5.80	6.56	0.61	0.53	<u>25.54</u>
	3PT _{svu}	0.71	1.95	0.88	0.73	25.70	0.39	0.92	0.91	0.85	27.43
Depth Pro [9]	P3P	0.71	1.95	0.88	0.73	17.48	0.40	0.90	0.92	0.86	18.02
	Rel3PT	13.13	26.01	0.39	0.27	<u>18.80</u>	3.03	5.28	0.66	0.58	28.27
	3PT _{svu}	<u>0.72</u>	<u>2.02</u>	<u>0.88</u>	<u>0.73</u>	25.10	<u>0.40</u>	<u>0.97</u>	<u>0.91</u>	<u>0.85</u>	<u>27.30</u>
UniDepth [49]	P3P	0.67	1.81	0.90	0.75	19.38	<u>0.39</u>	<u>0.90</u>	0.93	0.87	18.67
	Rel3PT	9.21	19.55	0.43	0.32	<u>26.38</u>	1.06	2.54	0.74	0.66	34.91
	3PT _{svu}	<u>0.68</u>	<u>1.84</u>	<u>0.90</u>	<u>0.74</u>	27.48	0.37	0.90	<u>0.92</u>	<u>0.86</u>	<u>27.16</u>
Metric3d V2 [27]	P3P	0.69	1.91	0.89	0.73	18.06	0.36	0.83	0.93	0.87	18.37
	Rel3PT	5.19	12.14	0.54	0.39	26.53	0.45	1.18	0.85	0.79	40.98
	3PT _{svu}	<u>0.71</u>	<u>1.98</u>	<u>0.88</u>	<u>0.73</u>	<u>25.17</u>	<u>0.38</u>	<u>0.93</u>	<u>0.92</u>	<u>0.86</u>	<u>27.23</u>
Marigold [31]	P3P	<u>0.73</u>	<u>2.06</u>	<u>0.86</u>	<u>0.70</u>	16.75	0.41	<u>1.10</u>	<u>0.86</u>	<u>0.80</u>	16.55
	Rel3PT	3.33	8.58	0.60	0.43	25.58	4.95	5.29	0.61	0.53	<u>26.13</u>
	3PT _{svu}	0.72	2.00	0.88	0.73	<u>24.27</u>	<u>0.42</u>	1.00	0.90	0.85	26.64
Marigold + FT [44]	P3P	<u>0.73</u>	<u>2.05</u>	<u>0.86</u>	<u>0.70</u>	16.46	<u>0.43</u>	<u>1.11</u>	<u>0.86</u>	<u>0.80</u>	16.53
	Rel3PT	3.35	8.49	0.60	0.44	25.69	4.98	4.77	0.61	0.54	26.70
	3PT _{svu}	0.72	1.99	0.88	0.73	<u>24.77</u>	0.41	1.08	0.91	0.85	<u>26.63</u>
MoGe [59]	P3P	0.67	1.83	0.90	0.74	18.53	<u>0.37</u>	<u>0.89</u>	0.93	0.87	18.38
	Rel3PT	5.91	13.17	0.54	0.37	28.70	3.72	5.16	0.63	0.54	29.27
	3PT _{svu}	<u>0.68</u>	<u>1.88</u>	<u>0.89</u>	<u>0.74</u>	<u>27.08</u>	<u>0.37</u>	0.81	<u>0.92</u>	<u>0.87</u>	<u>27.06</u>
Mean	P3P	<u>0.74</u>	<u>2.07</u>	<u>0.86</u>	<u>0.71</u>	17.16	<u>0.41</u>	<u>0.98</u>	<u>0.90</u>	<u>0.84</u>	17.56
	Rel3PT	6.03	12.81	0.56	0.41	28.78	3.40	4.01	0.69	0.62	32.69
	3PT _{svu}	0.70	1.95	0.88	0.73	<u>25.91</u>	0.40	0.95	0.91	0.85	<u>27.48</u>

Table 7. Rotation and translation errors (in degrees), and run-times (in milliseconds) on the Phototourism and ETH3D datasets for the calibrated problem with PoseLib [38]. The **best** and the second best methods are highlighted.

orientation. In *CVPR 2011*, pages 2969–2976. IEEE, 2011. 1

[34] Zuzana Kukelova, Martin Bujnak, and Tomas Pajdla. Closed-form solutions to minimal absolute pose problems with known vertical direction. In *Asian Conference on Computer Vision (ACCV)*, 2010. 2

[35] Zuzana Kukelova, Martin Bujnak, and Tomas Pajdla. Polynomial eigenvalue solutions to minimal problems in computer vision. *Trans. Pattern Analysis and Machine Intelligence (PAMI)*, 2012. 1, 3, 4

[36] Zuzana Kukelova, Jan Heller, and Andrew Fitzgibbon. Efficient intersection of three quadrics and applications in computer vision. In *Proceedings of the IEEE Conference on Computer Vision and Pattern Recognition*, 2016. 1

[37] Zuzana Kukelova, Joe Kileel, Bernd Sturmfels, and Tomas Pajdla. A clever elimination strategy for efficient minimal solvers. In *Computer Vision and Pattern Recognition (CVPR)*, 2017. 1, 5, 6

[38] Viktor Larsson and contributors. PoseLib - Minimal Solvers for Camera Pose Estimation, 2020. 8, 11, 13

[39] Viktor Larsson, Kalle Åström, and Magnus Oskarsson. Efficient solvers for minimal problems by syzygy-based reduction. In *Computer Vision and Pattern Recognition (CVPR)*, 2017. 3, 10

[40] Viktor Larsson, Zuzana Kukelova, and Yinqiang Zheng. Making minimal solvers for absolute pose estimation compact and robust. In *Proceedings of the IEEE International Conference on Computer Vision*, 2017. 1

[41] Hyon Lim, Sudipta N. Sinha, Michael F. Cohen, Matt Uyttendaele, and H. Jin Kim. Real-time Monocular Image-based

6-DoF Localization. *IJRR*, 34(4–5):476–492, 2015. 1

[42] Philipp Lindenberger, Paul-Edouard Sarlin, and Marc Pollefeys. Lightglue: Local feature matching at light speed. In *International Conference on Computer Vision (ICCV)*, 2023. 8

[43] Stephan Liwicki and Christopher Zach. Scale exploiting minimal solvers for relative pose with calibrated cameras. In *BMVC*, 2017. 2

[44] Gonzalo Martin Garcia, Karim Abou Zeid, Christian Schmidt, Daan de Geus, Alexander Hermans, and Bastian Leibe. Fine-tuning image-conditional diffusion models is easier than you think, 2024. 2, 7, 8, 12, 13

[45] Oleg Naroditsky, Xun S Zhou, Jean Gallier, Stergios I Roumeliotis, and Kostas Daniilidis. Two efficient solutions for visual odometry using directional correspondence. *Trans. Pattern Analysis and Machine Intelligence (PAMI)*, 2012. 2

[46] David Nistér. An efficient solution to the five-point relative pose problem. *Trans. Pattern Analysis and Machine Intelligence (PAMI)*, 2004. 1, 2, 3, 5, 7, 8

[47] Mikael Persson. *Visual Odometry in Principle and Practice*. PhD thesis, Linköping University Electronic Press, 2022. 1

[48] Mikael Persson and Klas Nordberg. Lambda twist: An accurate fast robust perspective three point (p3p) solver. In *Proceedings of the European conference on computer vision (ECCV)*, pages 318–332, 2018. 1

[49] Luigi Piccinelli, Yung-Hsu Yang, Christos Sakaridis, Mattia Segu, Siyuan Li, Luc Van Gool, and Fisher Yu. Unidepth: Universal monocular metric depth estimation. In *Proceedings of the IEEE/CVF Conference on Computer Vision and Pattern Recognition*, pages 10106–10116, 2024. 2, 7, 8, 9, 12, 13

[50] René Ranftl, Alexey Bochkovskiy, and Vladlen Koltun. Vision transformers for dense prediction. In *International Conference on Computer Vision (ICCV)*, 2021. 7, 8, 12, 13

[51] Paul-Edouard Sarlin, Cesar Cadena, Roland Siegwart, and Marcin Dymczyk. From coarse to fine: Robust hierarchical localization at large scale. In *Computer Vision and Pattern Recognition (CVPR)*, 2019. 1, 8

[52] Davide Scaramuzza and Friedrich Fraundorfer. Visual odometry [tutorial]. *IEEE robotics & automation magazine*, 2011. 1

[53] Johannes L Schonberger and Jan-Michael Frahm. Structure-from-motion revisited. In *Computer Vision and Pattern Recognition (CVPR)*, pages 4104–4113, 2016. 1

[54] Thomas Schops, Johannes L Schonberger, Silvano Galliani, Torsten Sattler, Konrad Schindler, Marc Pollefeys, and Andreas Geiger. A multi-view stereo benchmark with high-resolution images and multi-camera videos. In *Computer Vision and Pattern Recognition (CVPR)*, 2017. 7, 8

[55] Henrik Stewénius, David Nistér, Fredrik Kahl, and Frederik Schaffalitzky. A minimal solution for relative pose with unknown focal length. In *Computer Vision and Pattern Recognition (CVPR)*, 2005. 1

[56] Henrik Stewénius, Christopher Engels, and David Nistér. Recent developments on direct relative orientation. *ISPRS Journal of Photogrammetry and Remote Sensing*, 60(4):284–294, 2006. 1

[57] Linus Svärm, Olof Enqvist, Fredrik Kahl, and Magnus Oskarsson. City-scale localization for cameras with known vertical direction. *Trans. Pattern Analysis and Machine Intelligence (PAMI)*, 2016. 1

[58] Chris Sweeney, John Flynn, and Matthew Turk. Solving for relative pose with a partially known rotation is a quadratic eigenvalue problem. *International Conference on 3D Vision (3DV)*, 2014. 2

[59] Ruicheng Wang, Sicheng Xu, Cassie Dai, Jianfeng Xiang, Yu Deng, Xin Tong, and Jiaolong Yang. Moge: Unlocking accurate monocular geometry estimation for open-domain images with optimal training supervision, 2024. 2, 7, 8, 9, 12, 13

[60] Changchang Wu. P3. 5p: Pose estimation with unknown focal length. In *Proceedings of the IEEE Conference on Computer Vision and Pattern Recognition*, 2015. 1

[61] Lihe Yang, Bingyi Kang, Zilong Huang, Xiaogang Xu, Jiashi Feng, and Hengshuang Zhao. Depth anything: Unleashing the power of large-scale unlabeled data. In *Computer Vision and Pattern Recognition (CVPR)*, 2024. 2, 7, 8, 10, 12, 13

[62] Lihe Yang, Bingyi Kang, Zilong Huang, Zhen Zhao, Xiaogang Xu, Jiashi Feng, and Hengshuang Zhao. Depth anything v2. *arXiv preprint arXiv:2406.09414*, 2024. 2, 7, 8, 11, 12, 13

[63] Bernhard Zeisl, Torsten Sattler, and Marc Pollefeys. Camera pose voting for large-scale image-based localization. In *International Conference on Computer Vision (ICCV)*, 2015. 1